applied sciences

MDPI

Article

Study on Vibration-Transmission-Path Identification Method for Hydropower Houses Based on CEEMDAN-SVD-TE

Jianwei Zhang [1], Ziyu Li [1,*], Jinlin Huang [2], Mengran Cheng [1] and Huokun Li [3]

[1] School of Water Resources, North China University of Water Resources and Electric Power, Zhengzhou 450046, China; zhangjianwei@ncwu.edu.cn (J.Z.); 201621527@stu.ncwu.edu.cn (M.C.)
[2] Guangdong Research Institute of Water Resources and Hydropower, Guangzhou 510610, China; 201502622@stu.ncwu.edu.cn
[3] School of Civil Engineering and Architecture, Nanchang University, Nanchang 330031, China; lihuokun@ncu.edu.cn
* Correspondence: 201602416@stu.ncwu.edu.cn

Highlights:

- An new analysis method for vibration-transmission paths based on CEEMDAN-SVD-TE is proposed.
- It is verified that the CEEMDAN-SVD-TE method has higher effectiveness and is superior to the single TE algorithm.
- The feasibility of CEEMDAN-SVD-TE in practical engineering is verified by engineering examples from the Quxue hydropower house.
- By using the information-transmission rate, it is identified that the lower frame foundation is an essential node for vibration transmission.

Abstract: The analysis of the vibration-transmission path is one of the keys to the vibration control and safety monitoring of a hydropower house, and the vibration source of the hydropower house is complex, making it more difficult to analyze the vibration-transmission path. In order to accurately identify the transmission path of the vibration in a hydropower house, an identification method for the vibration-transmission path based on CEEMDAN-SVD-TE is presented in this paper. First of all, this paper verifies that the CEEMDAN-SVD-TE method has higher effectiveness and is superior to the single transfer-entropy (TE) algorithm in information-transmission-direction identification; secondly, based on the measured field-vibration data, CEEMDAN-SVD noise-reduction technology is used to adaptively decompose the characteristics according to the signal energy; finally, the transfer-entropy theory and the information-transmission rate are used to determine the vibration-transmission path of the hydropower house. The results show that the main transmission path of the vibration caused by tailwater fluctuation is tailwater pipe (top cover measurement point)→turbine pier (stator foundation measurement point, lower frame foundation measurement point)→generator floor (generator floor measurement point). This research can offer a reference for vibration control and safety monitoring of hydropower houses, and provide a new idea for structural vibration reduction.

Keywords: hydropower house; vibration-transmission path identification; CEEMDAN-SVD; transfer entropy

Citation: Zhang, J.; Li, Z.; Huang, J.; Cheng, M.; Li, H. Study on Vibration-Transmission-Path Identification Method for Hydropower Houses Based on CEEMDAN-SVD-TE. *Appl. Sci.* **2022**, *12*, 7455. https://doi.org/10.3390/app12157455

Academic Editor: Andrea Li Bassi

Received: 4 July 2022
Accepted: 22 July 2022
Published: 25 July 2022

Publisher's Note: MDPI stays neutral with regard to jurisdictional claims in published maps and institutional affiliations.

1. Introduction

Hydropower, as an important clean energy source, is receiving increasing attention from countries around the world [1–3]. The hydropower station, as an essential component of hydroelectric power generation, always has the mission of stability and safety of operation. The hydropower house is an important part of the hydropower station, which is not only the support structure of the hydro-generator unit, but also the channel for water to flow. With an increase in installed capacity and water head, the size of the

hydropower station becomes more significant and the stiffness gradually decreases, which leads to serious stability problems in a large hydropower house. Against this background, the vibration of the hydropower house structure caused by various factors such as unit vibration and channel water flow is increasingly drawing attention [4–7]. Thus, using effective methods to analyze the structural vibration response of the hydropower house, identifying its vibration-transmission path and evaluating the stability of its vibration state are of great practical significance and engineering value.

The vibration system of hydropower units and the power house is a huge coupled hydraulic–mechanical–electromagnetic structural system, and the main sources of vibration include hydraulic, mechanical and electromagnetic factors [8,9]. The coupling effect of multiple sources creates huge difficulties and presents great challenges for research into vibration issues. The vibration prototype observation of the hydropower house structure based on the excitation of the working environment can obtain the required vibration parameters and response under the normal operation working conditions, but because the vibration signal of the hydropower house is a non-linear signal with varied noise, the information of the vibration characteristics is often drowned by the noise under the joint influence of multiple vibration sources, which affects the accuracy of the subsequent data analysis [10].

In view of the various difficulties mentioned above, there are three thorny and step-by-step challenges that need to be addressed before proceeding with the evaluation of the vibration stability of hydropower house: (1) How to reduce the influence of noise and extract the characteristic information in the vibration signal with the help of effective methods; (2) How to effectively identify the transmission path of vibration energy during the operation of the hydropower house; (3) How to quantitatively evaluate the transmission strength of vibration energy and make recommendations for the optimization of the structure of the hydropower house.

In the field of signal processing, many studies have been conducted and many achievements have been made. The Fourier transform has been extensively applied in the field of signal processing, which not only can clarify the spectral features of signals, but also has the capability for precise resolution [11,12]. It is an effective tool for analyzing smooth signals but cannot correct and analyze local distortion of the signal. A digital filter is an improved Fourier-transform-based denoising method, which achieves denoising by mathematical operations on the difference equations of a discrete signal, but requires predefined technical specifications such as a passband cutoff frequency and stopband cutoff frequency [13,14]. The wavelet transform allows local transformation of the time and frequency of the signal, but there is no standard available for choosing the wavelet base function [15]. Empirical mode decomposition (EMD) is an adaptive signal-analyzing method for processing nonlinear and non-stationary signals [16,17]. Barbosh [18] introduces the application of the EMD method in complex vibration signal processing and modal identification of civil structures in detail. However, due to the defects of his computational theory, the decomposition process of EMD may cause boundary effects and mode mixing [19,20]. In order to reduce the interference of the mode mixing, the ensemble empirical mode decomposition (EEMD) method is proposed [21]. Spinosa [22] uses the EEMD method to effectively reduce the background noise of airframe-vibration data obtained from aircraft water-landing experiments. Gao [23] uses the EEMD method to extract weak fault signals from bearing vibration signals to achieve early bearing fault prediction. However, the effect of EEMD decomposition depends on the integration time and the amplitude of the added white noise [24]; the mode-mixing phenomenon will not be mitigated if the parameters are not chosen properly. With the purpose of overcoming the above problems, complete ensemble empirical mode decomposition with adaptive noise (CEEMDAN) is proposed. This method adds adaptive white noise at each stage of the decomposition and calculates a unique residual signal for each mode component, which results in negligible reconstruction error [25,26]. Mousavi [27] applies CEEMDAN to bridge structural vibration signal processing to effectively identify the location and extent of bridge damage. However, although CEEMDAN can effectively

decompose the signal and obtain the characteristic mode components, it cannot effectively filter out high-frequency white noise due to background noise [28]. Singular value decomposition (SVD), as a typical orthogonal decomposition denoising method, can efficiently filter out high-frequency noise in the signal [29].

As the problem of vibration in a hydropower house has become a subject of increasing concern, researchers have started to analyze vibration from the perspective of the vibration mechanism and have tried to explore the energy-transfer path of vibration in a hydropower house. Xu [30] studies the power transmission between the underground main powerhouse and auxiliary powerhouse based on the tidal current theory. They find that the vibration-transfer direction of the underground plant is mainly perpendicular to and along the flow direction of the bedrock. Lian [31] concludes that the transmission of transverse vibration was larger than that of longitudinal and vertical vibration, while the transmission intensity of low-frequency vibration and rotational frequency vibration were basically equal. Wang [32] carries out the calculation of structural sound intensity based on finite element theory for different parts of the hydropower plant, and realizes the vector visualization of the transmission path. Researchers often study the vibration of the hydropower house through numerical model calculations and have achieved good results, but the shortcomings and challenges cannot be ignored. Most previous studies have used computational analysis methods that assume the excitation of the house is usually composed of steady-state harmonic loads, which simplifies mathematical calculations but adds human interference.

In the field of vibration response analysis with the help of structural monitoring data, the transfer entropy (TE) has been widely used. Lindner [33] uses Granger causality and transfer entropy to analyze the vibration of the site and finds that transfer entropy can determine the cause and effect of the vibration more accurately. Wang [34] and Wang [35] have also attempted to investigate the structural response by the transfer entropy based on data acquired from field tests rather than numerical simulations. Zhang [36] applies the transfer entropy to the vibration-response analysis of the powerhouse structure to describe the vibration-transfer energy characteristics of different variables and the same variable in different directions. In this research, transfer entropy is introduced and verified as an innovative method that can analyze vibration-transmission paths based on structural vibration response data. However, using vibration monitoring data directly from field tests, the analysis process may be affected by strong background noise, resulting in inaccurate analysis results.

Considering the above problems and the advantage of CEEMDAN, SVD and TE in signal-analysis work, this paper proposes a new vibration-transmission path identification method for hydropower houses based on CEEMDAN-SVD-TE. Firstly, the accuracy and superiority of CEEMDAN-SVD-TE, which is higher than TE in information-transmission-direction identification, is verified by simulation-signal analysis. A large hydropower house is taken as the research object, and the CEEMDAN-SVD method is used to extract the tailwater-fluctuation signal as the characteristic signal for the transmission-path analysis; finally, the vibration-transmission path of tailwater fluctuation is analyzed using the transfer-entropy theory, and the information-transmission rate between different measurement points is calculated. This research can offer a dependable theoretical basis and technical support for the identification of the vibration mechanism and optimization of structural vibration reduction in hydropower houses.

This article is structured as follows. Section 2 introduces the basic theory used in the following sections. Section 3 presents the simulation analysis of the method proposed in the paper. Section 4 shows the results for the analysis of the vibration-transmission path from the measured point signals in the hydropower house. Finally, this article is concluded in Section 5.

2. Materials and Methods

2.1. CEEMDAN Algorithm

EMD [16] can adaptively decompose the original signal into an intrinsic mode function (IMF) according to its own scale. However, due to the problem of EMD's own computing theory, mode mixing often occurs in its decomposition. EEMD [21] is an improvement on EMD; its calculation principle is to add the corresponding white noise to the original signal and eliminate the mode-mixing phenomenon in EMD decomposition at one time by suppressing and canceling the influence of decomposition noise through multiple integration. After multiple integration averaging, the influence of white noise on the decomposition results is offset, but a reconstruction error appears. The reconstruction error relies on the integration number, and increasing the integration number can diminish the reconstruction error, but it increases the computational volume to some extent and seriously affects the computational efficiency.

In order to solve the problems of mode mixing, calculation accuracy and computational efficiency, the CEEMDAN algorithm is proposed. Compared with the EEMD algorithm, the CEEMDAN algorithm adds a finite amount of adaptive white noise at each stage of EMD decomposition. When the number of integrations is small, its reconstruction error is almost zero, and the reconstructed signal is almost identical to the original signal. Therefore, the CEEMDAN algorithm can solve the mode-mixing phenomenon existing in the EMD algorithm and overcome the incompleteness as well as low computational efficiency of the EEMD algorithm.

Define an operator $E_k(\cdot)$ that represents the process of EMD obtaining the k-th mode component IMF_k; let $\omega^i(t)$ be the white-noise-satisfying distribution of $N(0,1)$ and ε_k is the amplitude coefficient of white noise added for the k-th time. The decomposition process for the CEEMDAN algorithm is shown below [25]:

(1) The white noise $X(t) + \varepsilon_0\omega^i(t)$ is added to the original signal, and I-th EMD decomposition is performed. An average operation is then performed on the result to obtain IMF_1.

$$\mathrm{IMF}_1 = \frac{1}{I}\sum_{i=1}^{1} E_1(X(t) + \varepsilon_0\omega^i(t)) \tag{1}$$

(2) The first stage residual component can be calculated.

$$r_1(t) = X(t) - \mathrm{IMF}_1 \tag{2}$$

The white noise $r_1(t) + \varepsilon_1 E_1\left(\omega^i(t)\right), i = 1, 2, \ldots, I$ is added to the first-stage residual component, and the EMD is performed.

IMF_2 can then be calculated with the mean value of the first IMF.

$$\mathrm{IMF}_2 = \frac{1}{I}\sum_{i=1}^{1} E_1\left(r_1(t) + \varepsilon_1 E_1\left(\omega^i(t)\right)\right) \tag{3}$$

For $k = 1,\ 2,\ \ldots, K$, the k-th residual component can be calculated.

$$r_k(t) = r_{k-1}(t) - \mathrm{IMF}_k \tag{4}$$

(3) White noise $r_1(t) + \varepsilon_1 E_1\left(\omega^i(t)\right), i = 1, 2, \ldots, I$ is added to the k-th residual component and EMD decomposition performed. IMF_{k+1} can then be calculated with the mean value of the first IMF.

$$\mathrm{IMF}_{k+1} = \frac{1}{I}\sum_{i=1}^{1} E_1\left(r_k(t) + \varepsilon_k E_k\left(\omega^i(t)\right)\right) \tag{5}$$

(4) Step (4) and Step (5) are repeated until the value of the residual component is less than two extremes, then the decomposition stops. Eventually the residual variable is obtained.

$$r(t) = X(t) - \sum_{k=1}^{K} \mathrm{IMF}_k \tag{6}$$

where K is the total number of modes in the decomposition process.

The reconstructed signal can be expressed as follows:

$$X(t) = r(t) + \sum_{k=1}^{K} \mathrm{IMF}_k \tag{7}$$

2.2. SVD Denoising Algorithm

Singular value decomposition (SVD) is a classical noise-reduction method, which is widely used in vibration signal processing [29].

Assuming the signal $X = [x(1), x(2), \cdots x(n+m-1)]$, the Hankel matrix can be constructed as follows [37]:

$$H = \begin{pmatrix} x(1) & x(2) & \cdots & x(n) \\ x(2) & x(3) & \cdots & x(n+1) \\ \vdots & \vdots & & \vdots \\ x(m) & x(m+1) & \cdots & x(n+m-1) \end{pmatrix} \tag{8}$$

where H is the matrix of $m \times n$, $m \geq n$.

The singular value decomposition of H can be obtained. For any $m \times n$ orders real matrix H, there must be an orthogonal matrix $U \in R_{m \times m}$ and an orthogonal matrix $V \in R_{n \times n}$ to meet Equation (9).

$$H = UDV^T \tag{9}$$

where $U \in R_{m \times m}$; $V \in R_{n \times n}$; $D = (diag(\sigma_1, \sigma_2, \cdots, \sigma_p), 0)$ or its transpose; 0 denotes the zero matrix; σ_i represents the singular value obtained by decomposition, and satisfies $\sigma_i \geq \sigma_{i+1}$.

Assuming the optimal singular value order is r, the denoised signal $X = [x(1), x(2), \cdots x(n+m-1)]$ can be obtained by preserving the r order singular value of the singular value matrix D and reconstructing the matrix. The key problem is to determine the optimal order of singular value. If selected order is too low, the valid signal may be mistaken as noise, resulting in the loss of the valid signal. If selected order is too high, there will be a lot of residual noises, which affects the de-noising effect. The optimal order should preserve the valid signal in the maximal degree and filter out most of the noise.

A singular entropy increment is applied to identify the optimal order in this paper [28]; the order when the singular entropy increment curve tends to be steady is chosen for the optimal singular value order r, which ensures that the signal features are preserved and the unfavorable noise is filtered effectively.

2.3. Transfer-Entropy Algorithm

Schreiber [38] drew lessons from the basic theory of information entropy and extended it to form the transfer-entropy (TE) algorithm, which can characterize the relevance and information-transmission relationship among different time series with a unit of bit. This theory can quantify the information-transmission effect between related time series in the form of entropy and reflect the characteristics of information transmission. If the dynamic probabilities of a process x at time $n+1$ is conditional only on previous k values, the process is called a k-th Markov process. The mathematic description of this transition probability is

$$p(x(n+1) \mid x(n), x(n-1), \ldots, x(n-k+1)) = p\left(x(n+1) \mid x(n)^{(k)}\right) = p\left(x(1) \mid x^{(k)}\right) \tag{10}$$

Considering the influence of another process $y(m)^{(l)}$ on these transition probabilities, the expression of coupling influence of $x(n)^{(k)}$ and $y(n)^{(l)}$ on $x(n+1)$ is $p\left(x(1) \mid x^{(k)}, y^{(l)}\right)$.

The transfer entropy $T_{y\to x}\left(x(1) \mid x^{(k)}, y^{(l)}\right)$ can be formulated as below.

$$\begin{aligned} &T_{y\to x}\left(x(1) \mid x^{(k)}, y^{(l)}\right) \\ &= \iiint p\left(x(1), x^{(k)}, y^{(l)}\right) \log_2\left(\frac{p\left(x(1)|x^{(k)}, y^{(l)}\right)}{p\left(x(1)|x^{(k)}\right)}\right) \\ &\times dx(1)dx^{(k)}dy^{(l)} \end{aligned} \tag{11}$$

When the transfer entropy of y to x is greater than the transfer entropy of x to y, y is referred to as the source of information transmission and $T_{y\to x}\left(x(1) \mid x^{(k)}, y^{(l)}\right)$ denotes the transfer entropy of y to x. The research of Nichols and Overbey [39,40] showed that defining the order $k = l = 1$ for both Markov processes y and x does not affect the directedness of process y to process x. Together with a time delay τ added to $y(n)$, Equation (11) can be simplified to Equation (12).

$$\begin{aligned} &T_{y\to x}(x(1)|x, y(\tau))y(n) \\ &= \iiint p(x(1), x, y(\tau)) \log_2\left(\frac{p(x(1)|x, y(\tau))}{p(x(1)|x)}\right) \\ &\times dx(1)dxdy(\tau) \end{aligned} \tag{12}$$

where $y(\tau) \equiv y(n+\tau)$. The assumption of order $k = l = 1$ quantifies the information gain from $y(t)$ only.

If we use conditional probabilities $p(a|b) = p(a,b)/p(b)$, Equation (12) can be rewritten in entropy form as Equation (13).

$$\begin{aligned} &T_{y\to x}(x(1)|x, y(\tau)) \\ &= \iiint p(x(1), x, y(\tau)) \log_2 p(x(1), x, y(\tau))dx(1)dxdy(\tau) \\ &+ \int p(x) \log_2 p(x)dx - \iint p(x, y(\tau)) \log_2 p(x, y(\tau))dxdy(\tau) \\ &- \iint p(x(1), x) \log_2 p(x(1), x)dx(1)dx \end{aligned} \tag{13}$$

In order to quantitatively describe the transmission regularity of vibration energy, the information-transmission rate (ITR) index is introduced [35,36], which is calculated based on the transfer entropy and can effectively describe the information-transmission strength of vibration energy. For vibration signals y and x, the ITR is:

$$ITR_{y\to x} = \frac{\overline{T_{y\to x}(\tau)} - \overline{T_{x\to y}(\tau)}}{\overline{T_{y\to x}(\tau)}} \tag{14}$$

where $T_{y\to x}(\tau)$ and $T_{x\to y}(\tau)$ are the transfer entropy corresponding to the different transfer directions of signals x and y; $\overline{T_{y\to x}(\tau)}$ and $\overline{T_{x\to y}(\tau)}$ are the average value of $T_{y\to x}(\tau)$ and $T_{x\to y}(\tau)$, respectively; $ITR_{y\to x}$ is the information-transmission rate; the direction of $ITR_{y\to x} > 0$ is used as the positive direction of information transmission.

In the case of $T_{y\to x} - T_{x\to y} \geq 0$, when $ITR_{y\to x} = 0$, there is no information-transmission relationship between signal y and x, and the two signals are independent; When $ITR_{y\to x} = 1$, the information of signal y is completely transmitted to the signal$x$, y is the source of information transmission. Therefore, $ITR_{y\to x}$ can describe the information-transmission intensity of $y \to x$ in the form of percentage, so as to quantitatively characterize the feature of information transmission between vibration signals.

2.4. COMBINED CEEMDAN-SVD-TE

The vibration signal of a hydropower house is a kind of nonlinear and non-stationary signal, including high-frequency white noise and electromagnetic noise. The CEEMDAN algorithm can effectively extract the required feature signal according to frequency, but

because of the interference of strong background noise, a lot of high-frequency white noise cannot be separated accurately. To ensure the accuracy of feature-information extraction, the vibration signal needs to be further processed. As a classical denoising method, the SVD algorithm has a strong ability to filter the high-frequency random noise in the signal and extract the signal-feature information. The transfer-entropy algorithm can effectively analyze the correlation between signals, identify the source of information transmission and clarify the direction of vibration-signal transmission.

Based on the working characteristics of the hydropower house and the advantages of each method, the CEEMDAN-SVD-TE method is introduced in this paper. The flow chart of the CEEMDAN-SVD-TE is presented in Figure 1, and the principal procedures can be summarized as follows:

(1) The collected vibration signal is decomposed to IMFs from high frequency to low frequency by CEEMDAN processing, and the IMF component can represent the vibration characteristics of the structure.
(2) The optimal singular value order r is selected according to the singular entropy increment theory, and the high-frequency noise in the IMF signal is filtered out utilizing the singular value decomposition algorithm.

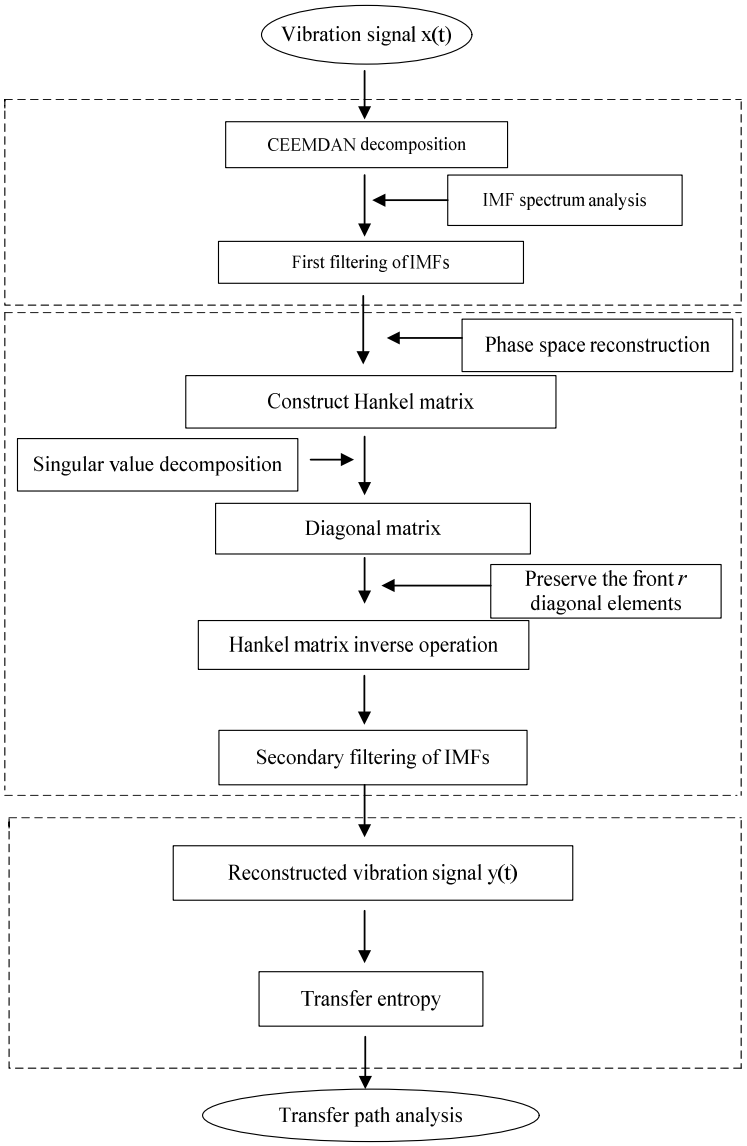

Figure 1. Flow chart of the CEEMDAN-SVD-TE method.

(3) The IMF component is reconstructed by CEEMDAN-SVD joint filtering, and the target feature signal is obtained.
(4) The reconstructed feature signals are analyzed for transfer effects with the help of the transfer-entropy algorithm to identify the direction of information transmission between signals.

3. Simulation Analysis

3.1. CEEMDAN-SVD Simulation

To test the validity of the joint CEEMDAN-SVD filtering, a simulation signal $f(t)$ with superimposed low-frequency noise and high-frequency noise is constructed with sampling frequency $f = 100$Hz, sampling time $t = 10$ s. The equation is as follows:

$$f(t) = y(t) + y_1(t) + y_2(t) \tag{15}$$

Pure signal:

$$y(t) = 10e^{-t\pi/2}\sin(16t) + 5e^{-t/3}\sin(25t) \tag{16}$$

Low-frequency noise:

$$y_1(t) = 8e^{-t/3}\sin(3t) \tag{17}$$

High-frequency white noise:

$$y_2(t) = 4randn(m) \tag{18}$$

where t is the time; m is the number of samples; $randn(m)$ is white noise.

A comparison of the time history for signals $f(t)$ and $y(t)$ is shown in Figure 2, and a comparison of the power spectral density plot is shown in Figure 3.

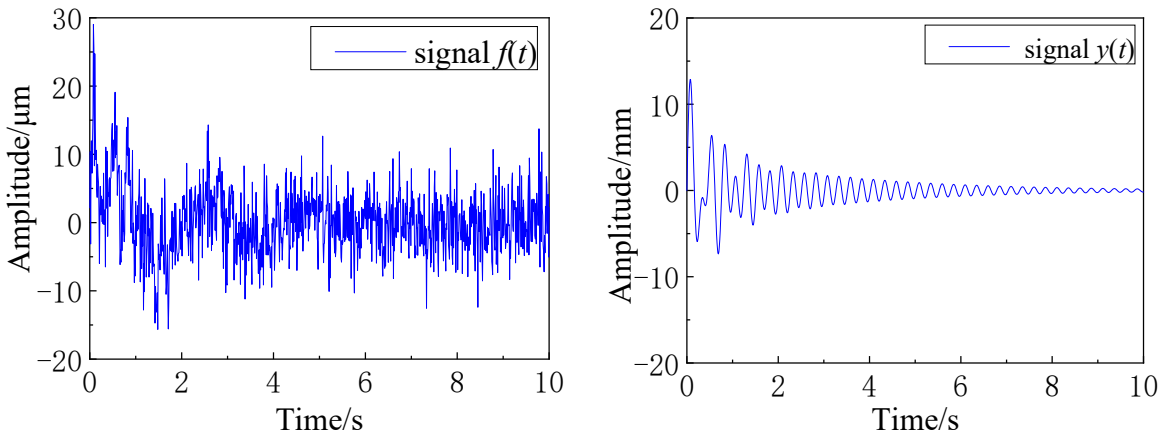

(**a**) (**b**)

Figure 2. Time history comparison of noised signal $f(t)$ and pure signal $y(t)$. (**a**) Time history of noised signal $f(t)$; (**b**) Time history of pure signal $y(t)$.

Because part of the true frequency of the pure signal will be masked by noise, the presence of noise will influence the accuracy of feature-information extraction. Filtering and denoising the acquired signal is the key step of signal analysis. In this paper, the SVD, EEMD, CEEMDAN and CEEMDAN-SVD methods are used to reduce the noise of $f(t)$, and the noise-reduced results of each method are compared to verify the good applicability of the CEEMDAN-SVD algorithm for noisy signal filtering.

The comparison of the power spectrum after noise reduction by the filtering methods are shown in Figure 4.

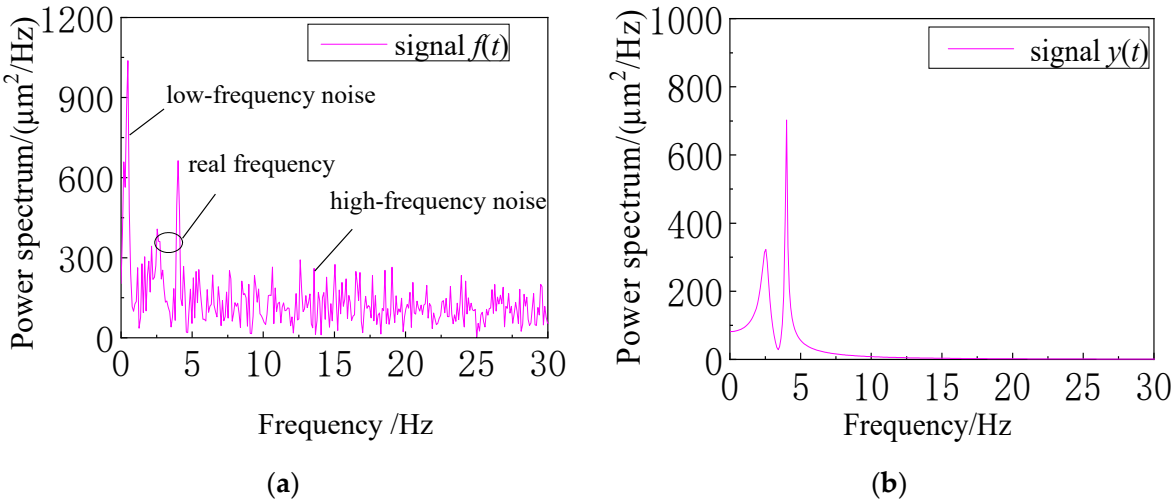

Figure 3. Power-spectrum comparison of noised signal $f(t)$ and pure signal $y(t)$. (**a**) Power spectrum of noised signal $f(t)$; (**b**) Power spectrum of pure signal $y(t)$.

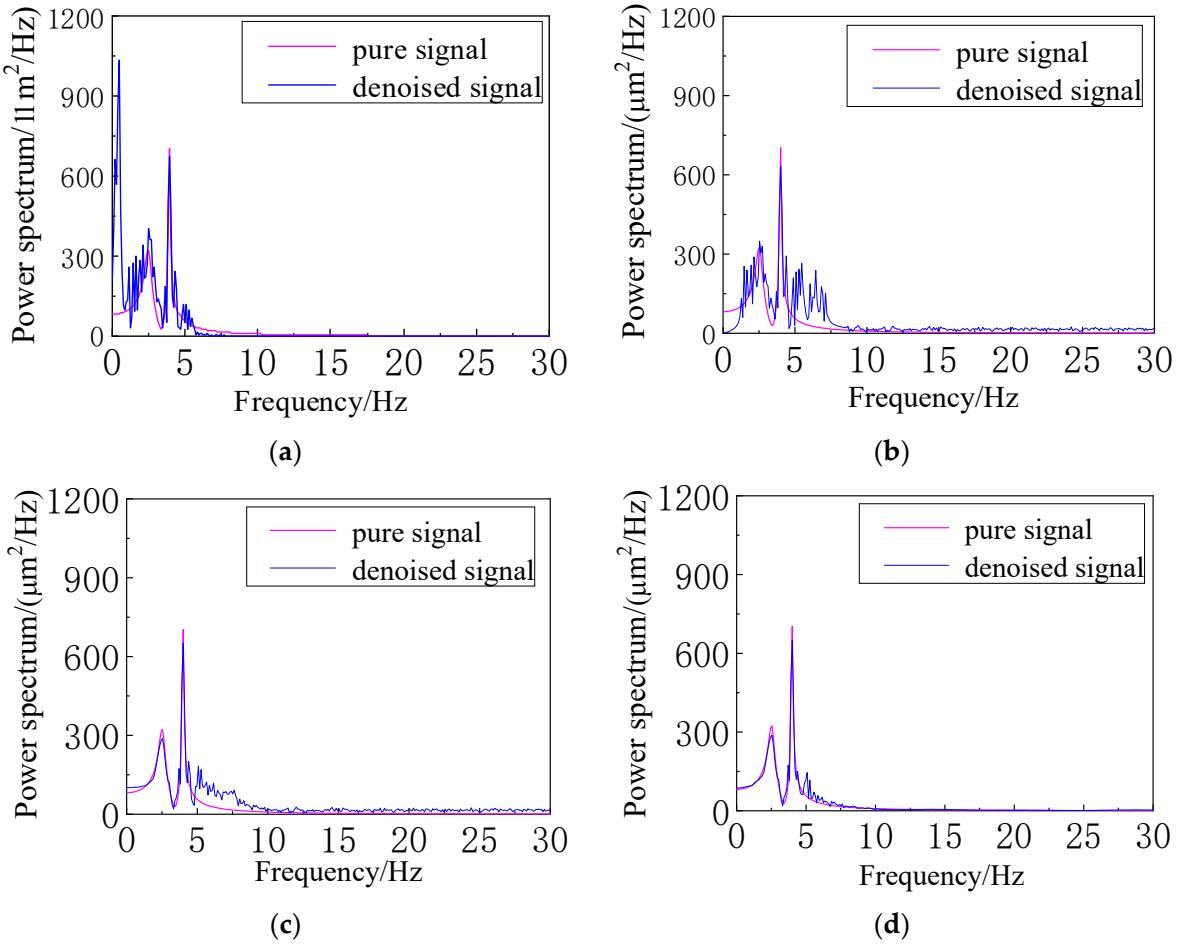

Figure 4. Power-spectrum comparison of four filtering methods for the noised signal $f(t)$. (**a**) Result of SVD; (**b**) Result of EEMD; (**c**) Result of CEEMDAN; (**d**) Result of CEEMDAN-SVD.

From Figure 4a, we can see that although the SVD algorithm can filter out the high-frequency noise in the original signal well, there is still a large amount of residual low-frequency noise. Figure 4b presents the filtering effect of EEMD, and its filtering accuracy is low because EEMD is greatly affected by background noise. In Figure 4c, the filtering

accuracy of CEEMDAN for high-frequency noise is low, but the effect of filtering low-frequency noise is excellent. From Figure 4d, CEEMDAN-SVD has a good filtering effect for both low-frequency and high-frequency noise.

Through the analysis of the filtering effect comparison, among the four filtering methods, CEEMDAN-SVD filter can effectively remove high-frequency noise while filtering low-frequency noise, and the accuracy of feature-signal extraction is higher than the other three methods, which can effectively extract the target signal.

To quantitatively evaluate the filtering capabilities of SVD, EEMD, CEEMDAN and CEEMDAN-SVD, the signal-to-noise ratio (*SNR*) and root mean square error (*RMSE*) are applied to assess the filtering capabilities of the above four methods.

$$SNR = lg\left\{\frac{\frac{1}{m}\sum_{i=1}^{m} f^2(m)}{\frac{1}{m}\sum_{i=1}^{m}\left[f(m)-\widehat{f(m)}\right]^2}\right\}^{10} \tag{19}$$

$$RMSE = \sqrt{\frac{1}{m}\sum_{i=1}^{m}\left[f(m)-\widehat{f(m)}\right]^2} \tag{20}$$

where $f(m)$ represents the original signal; $\widehat{f(m)}$ represents the signal after noise reduction.

If the *SNR* is larger and the *RMSE* is smaller, this shows that the denoising effect of this method is better. The denoising performance of SVD, EEMD, CEEMDAN and CEEMDAN-SVD are compared, as shown in Table 1.

Table 1. Comparison of *SNR* and *RMSE* results of four denoising methods.

Denoising Methods	*SNR*	*RMSE*
SVD	−2.04	2.38
EEMD	1.85	1.49
CEEMDAN	3.66	1.19
CEEMDAN-SVD	4.35	1.07

The two indexes calculated in Table 1 show that among the four methods of SVD, EEMD, CEEMDAN and CEEMDAN-SVD, the maximum *SNR* of CEEMDAN-SVD is 4.35 and the minimum *RMSE* is 1.07. According to the evaluation principles of *SNR* and *RMSE*, the CEEMDAN-SVD algorithm has the best denoising performance, indicating that the method can effectively filter out low-frequency noise and high-frequency noise and is more suitable for the analysis of low-*SNR* signals.

3.2. Transfer-Entropy Simulation

In order to apply the transfer-entropy algorithm to the analysis of the vibration-transmission path of the hydropower house, it is necessary to determine the efficiency of the transfer-entropy algorithm in the identification on the direction of information transmission.

Construct two correlated simulation signals A and B:

$$A = \cos(2\pi x_1 t) + 0.2\sin(2\pi x_2 t) \tag{21}$$

$$B = \mu A + 0.1\cos(2\pi x_1 t)\cos(2\pi x_2 t) - \cos(2\pi x_2 t) \tag{22}$$

where $x_1 = 40$; $x_2 = 4$; μ is the correlation coefficient.

As shown in Equations (21) and (22), it can be seen that the signal B consists of the signal A with correlation coefficient μ and part of the interference signal. From the perspective of the signal composition, as the correlation coefficient μ increases, the proportion of signal A in signal B increases and the proportion of interference signal decreases. The signal A should be more easily considered as the source of the B signal. On the basis of this,

this section identifies the applicability of transfer entropy in the direction identification and quantitative analysis of transfer effects between signals by varying the correlation coefficient μ in the signal B and analyzing the changes in $T_{A\to B}$ and $T_{B\to A}$ with different correlation coefficients μ.

The correlation coefficients μ of signals A and B are set to 0.2, 0.4, 0.6 and 0.8, respectively, and the transfer entropy $T_{A\to B}$ and $T_{B\to A}$ between the simulated signals A and B is calculated. The curves of the transfer-entropy values with the change in time are shown in Figure 5 and the information-transmission rate with different correlation coefficients are shown in Table 2.

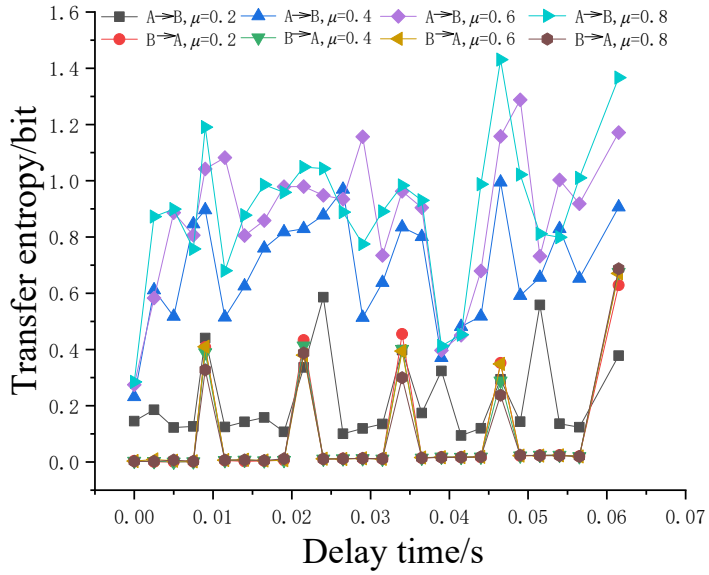

Figure 5. Transfer-entropy curve.

Table 2. The information-transmission rate of different correlation coefficients.

Correlation Coefficients μ	0.2	0.4	0.6	0.8
ITR/%	12.30	59.52	88.70	93.57

From Figure 5 and Table 2, the following conclusions can be drawn:

(1) When the correlation coefficient μ is 0.2, 0.4, 0.6, 0.8, $T_{A\to B}$ are all greater than $T_{B\to A}$, indicating that a large amount of information is transmitted from A to B, and the pure signal A is the source of information transmission. This is consistent with the actual simulation signal-information-flow direction; the B signal is constructed according to signal A and the signal A has no interference signals and has the main characteristics of the B signal. From the perspective of calculating transfer entropy, the amount of information flowing from A to B is much larger than that in the opposite direction, and more significant transfer effect can be obtained.

(2) When the correlation coefficient μ is 0.2, the values of $T_{A\to B}$ and $T_{B\to A}$ are close to each other, which is not conducive to the identification of the transmission direction between two signals, and $ITR_{A\to B}$ is 12.30%. As the correlation coefficient becomes larger, the difference between $T_{A\to B}$ and $T_{B\to A}$ becomes larger, and the transmission effect becomes more and more obvious. When the correlation coefficient μ is 0.8, $ITR_{A\to B}$ is 93.57%. This result indicates that the transfer entropy is highly sensitized to the transmission direction of the information flows between two signals, and the transfer-entropy curve can accurately reflect the direction of information transmission between two signals.

(3) In this section, simulation signals A and B are constructed, and the reasonableness of the transfer entropy for judging the direction of information transmission between two signals is verified by changing the magnitude of the correlation coefficient μ. $ITR_{A\to B}$

increases with the increasing correlation coefficient μ, which is consistent with the correlation of the constructed signals, indicating that the transfer entropy can not only reflect the directionality of information transmission between two signals, but also accurately quantify the correlation degree between the two signals from the perspective of entropy.

3.3. CEEMDAN-SVD-TE Simulation

To further study the possible influence of noise on the transfer-entropy calculation results and to clarify the usefulness of the joint CEEMDAN-SVD-TE method, the same set of Gaussian white noise was added to the signals A and B with correlation coefficient μ of 0.8; the signals A and B were noise-reduced with the help of CEEMDAN-SVD method, and the transfer-entropy curves of A and B signals before and after noise reduction were compared. Here, take the A signal as an example to show the effect of CEEMDAN-SVD noise reduction, the power spectrum of the A signal before and after noise reduction can be seen in Figure 6.

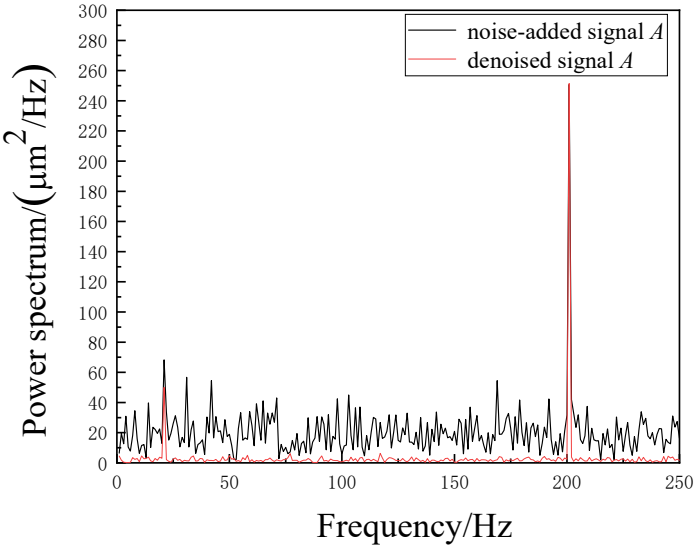

Figure 6. Comparison of the power spectrum before and after noise reduction for the noise-added signal A.

Figure 6 shows that the 25 Hz characteristic frequency of the signal after noise addition is drowned by the high-frequency white noise, and the high-frequency white noise in the original signal can be effectively filtered out with the help of the CEEMDAN-SVD method. After CEEMDAN-SVD noise reduction, the characteristic main frequencies of the pure signal (25 Hz and 200 Hz) are highlighted again.

The transfer-entropy curves of A and B before and after noise reduction are presented in Figure 7. As shown in the figure, without noise reduction of A and B, the values of $T_{A\to B}$ and $T_{B\to A}$ are interleaved and converge, indicating that the characteristic information of the signals may have been submerged by the high-frequency noise and the information-transmission effect between the signals is weakened. According to Table 2 and Figure 7, the $ITR_{A\to B}$ obtained from the signals of A and B without noise is 93.57%,the $ITR_{A\to B}$ obtained from the signals of A and B after noise reduction is 90.22%, and the $ITR_{A\to B}$ of A and B without noise reduction is 12.08%. These results indicate that the ITR can reflect the information-transmission strength between two signals, but the noise in the signals will weaken the transfer effect between the signals and have a negative effect on the computation results of transfer entropy. Using the CEEMDAN-SVD method can prevent the noise from the interference of the signal transmission direction analysis and effectively improve the accuracy of information-transmission-direction identification.

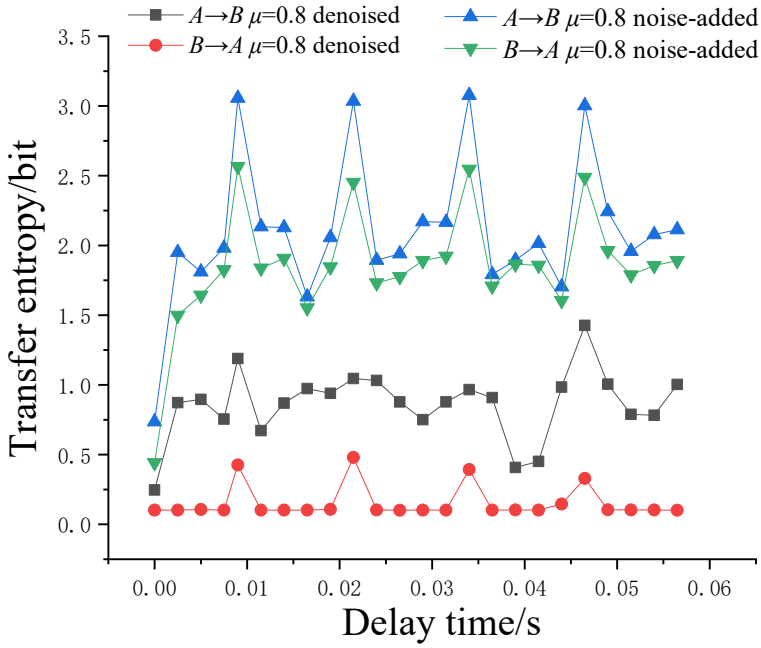

Figure 7. The transfer-entropy curves of *A* and *B* before and after noise reduction.

In summary, the transfer-entropy algorithm can effectively determine the transmission source of the signal, but its results are easily affected by noise signals. Integrating the CEEMDAN-SVD noise-reduction method with the transfer-entropy algorithm can effectively reduce the negative impact of noise on the transfer-entropy calculation results and obtain real and reliable transmission-path results.

4. Analysis of Transmission Path of Hydropower House

4.1. Project Summary

The Quxue hydropower house is located on Jinsha River in China, which is composed of structures for water retaining, discharge, water conveyance, an underground powerhouse and other buildings. The maximum hydraulic head is 210.3 m and the minimum hydraulic water head is 147.4 m.

The water-pressure fluctuation in the tailwater pipe and top-cover area is the main dynamic load of the unit and the structure's vertical vibration, and the low-frequency water-pressure fluctuation will cause the same frequency in the lower part of the top cover when it propagates upward in the hydraulic turbine. Therefore, the top-cover part can characterize the vibration of water turbulence in the tailwater pipe, the stator foundation and the lower frame foundation part can characterize the vibration of the turbine pier part and the generator floor part can characterize the vibration of the upper floor structure of the hydropower house.

On the basis of the above analysis, displacement sensors were arranged at the top cover, stator foundation, lower frame foundation and generator floor of the hydropower house. The vibration data were collected by 891-II vibration pickup and calibrated by INV9828 vibration pickup. The correspondence between the channel number and the location of the measurement points was as follows: 1—top cover; 2—lower frame foundation; 3—stator foundation; 4—generator floor.

The displacement sensor is shown in Figure 8. The measurement points are layout as shown in Figure 9.

The vibration excitation of the hydropower house structure is obtained under the instantaneous conditions of the unit start-up, shut-down and stable operation conditions of the machine. To assure the validity and completeness of the vibration signal analysis, three working conditions were set with a sampling frequency of 1024 Hz and a sampling time of 1000 s. The working conditions are shown in Table 3.

Figure 8. Displacement sensor.

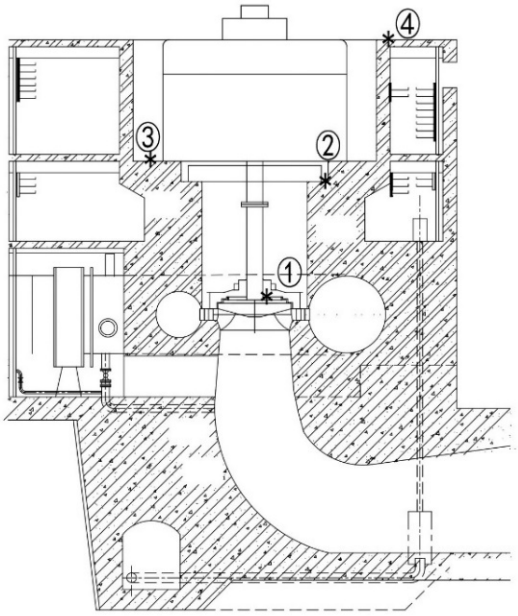

Figure 9. Layout of measuring points. (①—top cover; ②—lower frame foundation; ③—stator foundation; ④—generator floor).

Table 3. Test conditions of powerhouse of hydropower station.

No.	Test Conditions	Sampling Time/s	Sampling Frequency/Hz
1	Start-up Operation Condition of Hydropower Station Units	1000	1024
2	Stable Operation Condition of Hydropower Station Units	1000	1024
3	Shut-down Operation Condition Hydropower Station Units	1000	1024

4.2. Transmission Path Identification

4.2.1. Transmission Path Identification Process

In view of the complexity of the hydropower house vibration, the specific process of vibration-transmission-path identification is as follows:

(1) Collect the measured vibration information from different measurement points.
(2) Decompose the collected vibration-response signals into characteristic IMFs based on CEEMDAN theory.
(3) Select the optimal singular value order r with the help of singular entropy increment theory, and filter the noise of the decomposed IMFs with the help of SVD algorithm.
(4) Select the required target IMFs and perform feature-signal reconstruction.

(5) Calculate the transfer entropy of the feature signal between different measurement points with time, and plot the transfer-entropy curve.
(6) Analyze the transmission direction of the vibration signal and identify the vibration-transmission path of the hydropower house.

4.2.2. Operating Characteristic Information Extraction

The vibration sources of the hydropower house are composed of mechanical vibration, electromagnetic wave motion, and water-flow fluctuation. The vibration generated by water flow is the main source of hydropower house vibration. In order to clarify the vibration-transmission path of the hydropower house, it is necessary to pre-process the vibration signals collected by the pickups with the help of the CEEMDAN-SVD method before analyzing the vibration-signal-transmission direction with the help of the transfer-entropy algorithm. Here, taking the vibration signal collected at measurement point 1 of condition 2 as an example, the CEEMDAN-SVD is applied to decompose the signal for noise reduction. The time history and power spectrum of the vibration response of measurement point 1 under condition 2 are shown in Figures 10 and 11; the spectrum of singular entropy increment is shown in Figure 12.

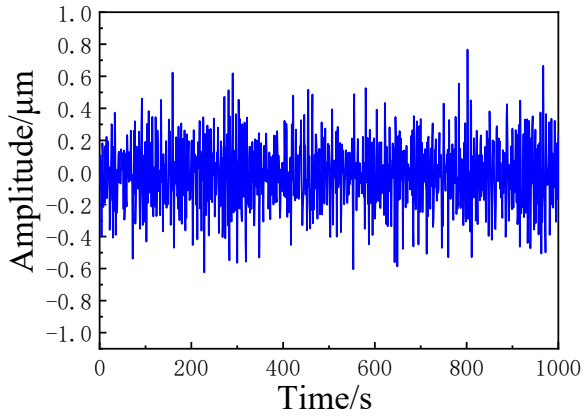

Figure 10. Time history of measurement point 1 under condition 2.

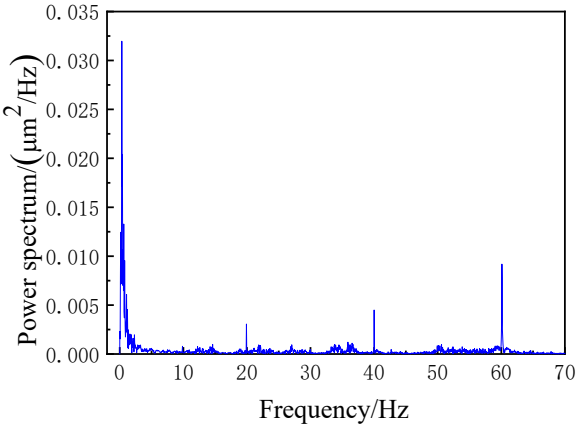

Figure 11. Power spectrum of measurement point 1 under condition 2.

From the power spectrum in Figure 11, the vibration response of measurement point 1 has four main frequency bands, 60 Hz, 40 Hz, 20 Hz and 0.5 Hz. The singular entropy increment curve is shown in Figure 12. According to the theory of singular entropy increment, the value of the singular entropy increment after the 70th order tends to be stable and is less than 0.03, which means that the singular value before 70th order already contains the main characteristic information of vibration signal, and the singular value

after 70th order is mostly caused by noise. Therefore, the optimal singular value order r is defined as 70.

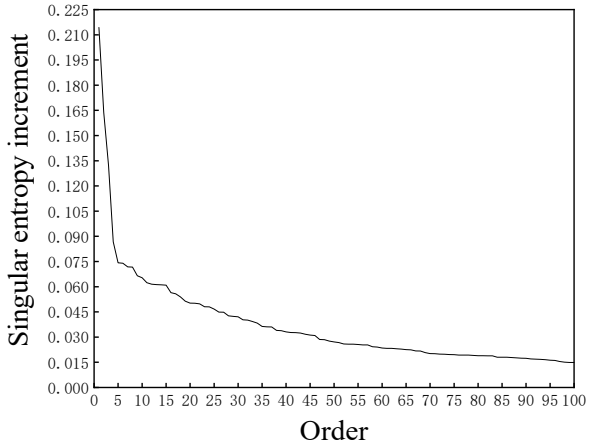

Figure 12. Singular entropy-increment curve.

The vibration response of measurement point 1 under condition 2 is processed by CEEMDAN-SVD and four IMFs are obtained; the IMFs are shown in Figure 13. The frequencies of IMF1-IMF4 correspond to the bands in Figure 11 (60 Hz, 40 Hz, 20 Hz, and 0.5 Hz), respectively. The vibration frequencies of 60 Hz, 40 Hz and 20 Hz correspond to the spike-power spectrum, and 0.5 Hz corresponds to the broad peak-power spectrum. The broad peak-power spectrum is the typical feature of a low-frequency water-flow signal; the vibration excitation band of 0.5 Hz corresponds to the water-flow fluctuation. The vibration of the hydropower house is mainly caused by water-flow fluctuation, so the IMF1 is retained as the required feature signal. With the help of CEEMDAN-SVD, the characteristic signal of water fluctuation is extracted from each measurement point and the vibration-transmission path of the hydropower house is analyzed on the basis of the water-fluctuation signal.

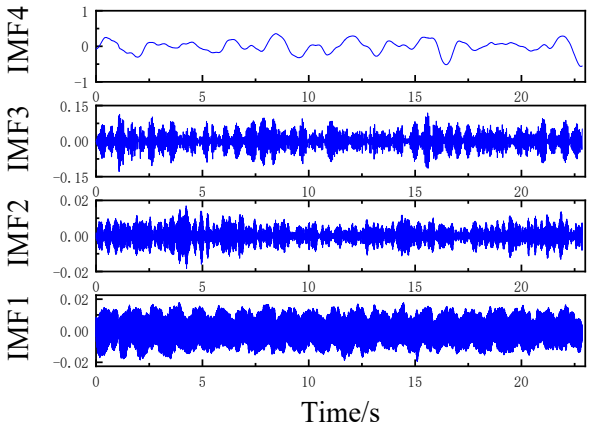

Figure 13. Time history of IMFs.

4.2.3. Analysis of Vibration-transmission Path under Start-Up Operation Condition of Hydropower Station Units

The transfer-entropy curve of the water-fluctuation signal at each measurement point under the start-up operation condition of the hydropower station unit is shown in Figure 14. The information-transmission rates between different measurement points are shown in Table 4.

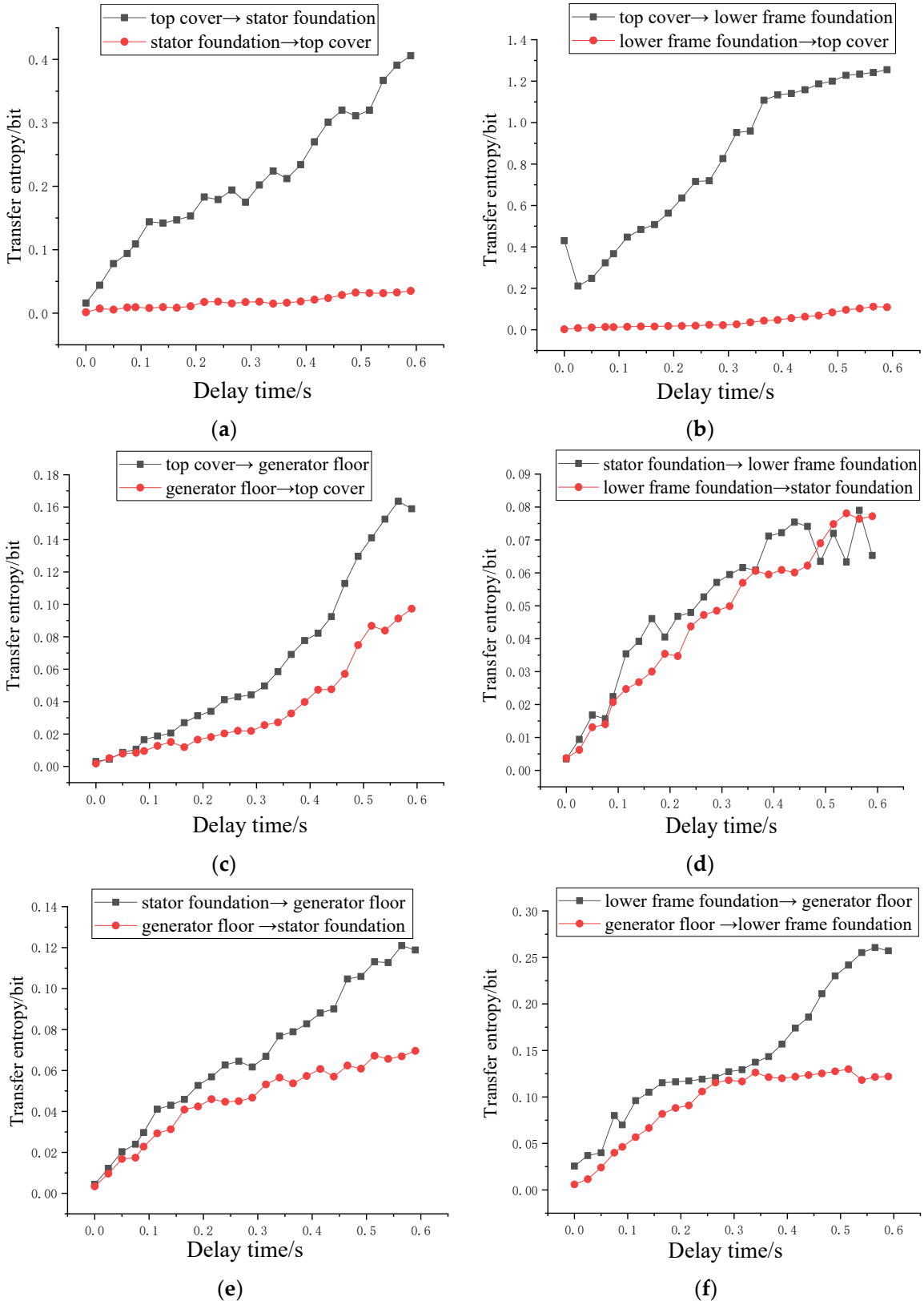

Figure 14. Transfer-entropy curve between measurement points of condition 1. (**a**) Transfer-entropy curve of top cover and stator foundation; (**b**) Transfer-entropy curve of top cover and lower frame foundation; (**c**) Transfer-entropy curve of top cover and generator floor; (**d**) Transfer-entropy curve of stator foundation and lower frame foundation; (**e**) Transfer-entropy curve of stator foundation and generator floor; (**f**) Transfer-entropy curve of lower frame foundation and generator floor.

Table 4. Information-transmission rate between measurement points of condition 1.

Transmission Direction	top cover→stator foundation	top cover→lower frame foundation	top cover→generator floor	stator foundation→lower frame foundation	stator foundation→generator floor	lower frame foundation→generator floor
ITR/%	91.54	94.86	44.55	9.35	32.85	32.78

From Figure 14a and Table 4, it can be observed that the transfer entropy from the top cover to the stator foundation is larger than that from the stator foundation to the top cover and the information-transmission rate is 91.54%, which means that a large amount of information flows from the top cover to the stator foundation, thus judging that the vibration-transmission direction is top cover→stator foundation; Similarly, from Figure 14b,c,e,f, it can be judged that the transfer directions of information are: top cover→stator foundation, top cover→lower frame foundation, stator foundation→generator layer floor, lower frame foundation→generator floor. The transfer entropy between the stator foundation and lower frame foundation measurement points in Figure 14d are close, the two transfer-entropy curves are staggered and the information-transmission rate is 9.35%, which means that there is no obvious one-way information effect between the two measurement points, so the information-transmission direction between the stator foundation and the lower frame foundation can be disregarded.

4.2.4. Analysis of Vibration-Transmission Path under Stable Operation Condition of Hydropower Station Units

The transfer-entropy curve of the water fluctuation signal at each measurement point under the stable operation condition of the hydropower station unit are shown in Figure 15. The information-transmission rate between different measurement points are shown in Table 5.

Comparing Figure 14 with Figure 15, it can be found that although the transfer-entropy curve under the start-up operation condition shows an obvious rising trend and the transfer-entropy curve under the stable operation condition shows a fluctuating trend, the vibration-transmission direction between the measurement points of the two conditions is identical, indicating that the vibration form of the hydropower house has not changed, and the vibration transfer directions are top cover→stator foundation, top cover→lower frame foundation, stator foundation→generator layer floor, lower frame foundation→generator floor.

Comparing Tables 4 and 5, it can be found that the information-transmission rate of stator foundation→generator floor and lower frame foundation→generator floor under the stable operation condition is greater than the start-up condition, which indicates that the vibration caused by the fluctuation of the tail water during the stable operation of hydropower station units has a greater impact on the upper structure of the hydropower house.

Table 5. Information-transmission rate between measurement points of condition 2.

Transmission Direction	top cover→stator foundation	top cover→lower frame foundation	top cover→generator floor	stator foundation→lower frame foundation	stator foundation→generator floor	lower frame foundation→generator floor
ITR/%	64.72	82.19	52.04	3.14	73.95	55.23

4.2.5. Analysis of Vibration-Transmission Path under Shut-down Operation Condition of Hydropower Station Units

The transfer-entropy curve of the water fluctuation signal at each measurement point under the shut-down operation condition of the hydropower station unit are shown in Figure 16. The information-transmission rate between different measurement points is shown in Table 6.

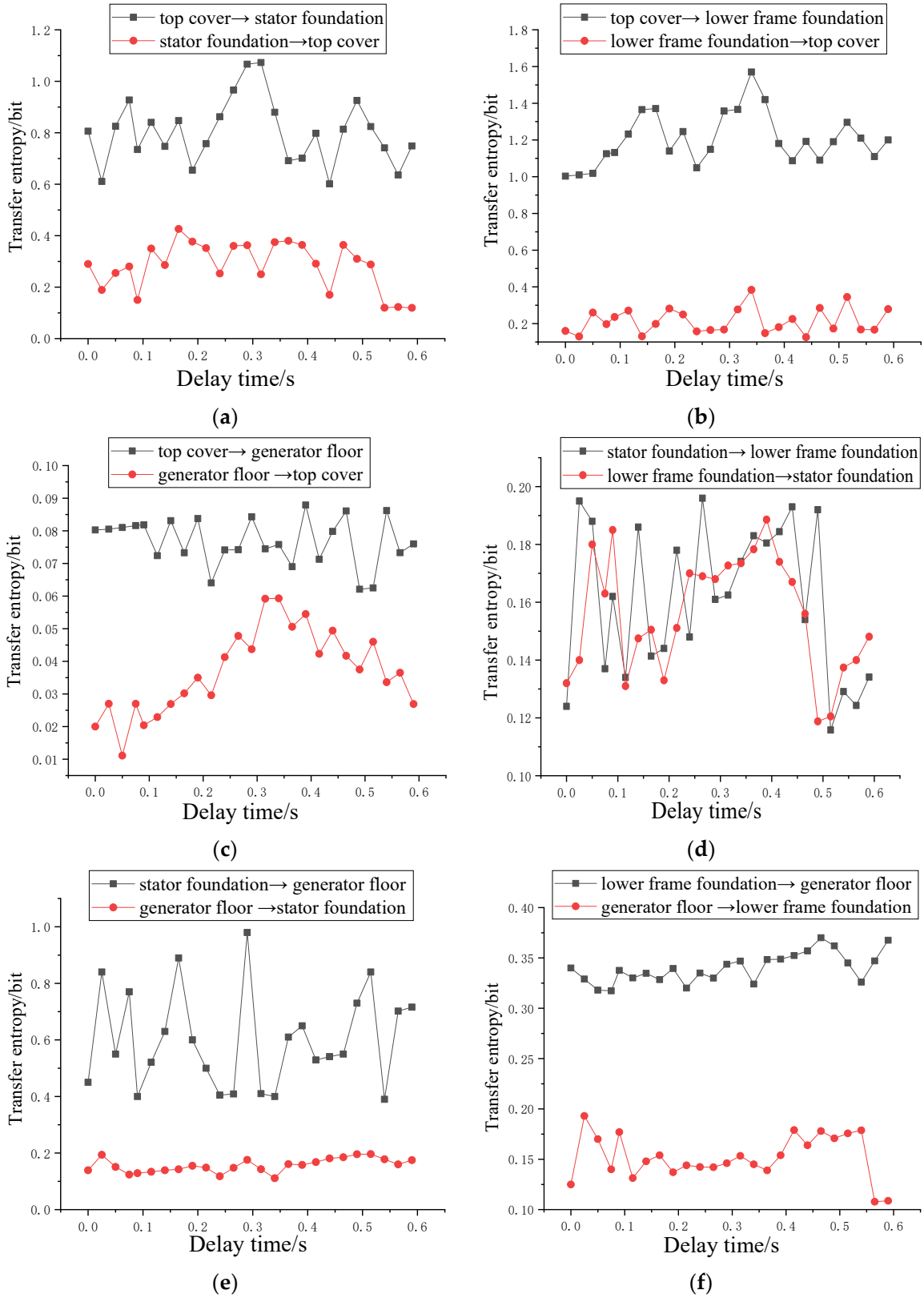

Figure 15. Transfer-entropy curve between measurement points of condition 2. (**a**) Transfer-entropy curve of top cover and stator foundation; (**b**) Transfer-entropy curve of top cover and lower frame foundation; (**c**) Transfer-entropy curve of top cover and generator floor; (**d**) Transfer-entropy curve of stator foundation and lower frame foundation; (**e**) Transfer-entropy curve of stator foundation and generator floor; (**f**) Transfer-entropy curve of lower frame foundation and generator floor.

Table 6. Information-transmission rate between measurement points of condition 3.

Transmission Direction	top cover→stator foundation	top cover→lower frame foundation	top cover→generator floor	stator foundation→lower frame foundation	stator foundation→generator floor	lower frame foundation→generator floor
ITR/%	71.67	72.99	65.23	4.04	47.62	29.97

As shown in Figure 16, under the shut-down condition, the transfer entropy between the measurement points decreases continuously, indicating that the information-transfer effect between the measurement points is weakening, but the transmission direction of vibration remains unchanged, and the transmission paths of the vibration are still top cover→stator foundation, top cover→lower frame foundation, stator foundation→generator layer floor, lower frame foundation→generator floor.

From Table 6, we can find that the information-transmission rate of top cover→stator foundation is 71.67%, and the information-transmission rate of top cover→lower frame foundation is 72.99%, which means that a large amount of vibration energy is transferred from the top cover. Comparing Tables 4–6, we can find that the information-transmission rate of top cover to stator foundation and lower frame foundation is significantly higher than that of other measurement points under the three working conditions, and the information-transmission rate of top cover→lower frame foundation is consistently the largest.

4.2.6. Results

The information-transmission rate between the main measurement points under three conditions is summarized in Table 7. Through the comparative analysis of the transfer-entropy curve and the information-transmission rate of the three working conditions in Table 7, the following conclusions can be drawn:

(1) Taking the calculation results of transfer entropy and the information-transmission rate of the start-up operation condition as an example to analyze the vibration form of the hydropower house, under the start-up operation condition, the information-transmission rate between the top cover and the lower frame foundation is 94.86%, and that from the top cover to the stator foundation is 91.54%, indicating that a larger part of the energy of the top cover is transferred to the turbine pier. The information-transmission rate from the stator foundation to the generator floor is 32.85%, and the information-transmission rate from the lower frame foundation to the generator floor is 32.78%, indicating that the vibration-transfer strength of the turbine pier and the generator floor is smaller than that of the top cover and the turbine pier. Considering the internal structure of the hydropower station, it is presumed that the main reason for reducing the vibration transfer effect is the energy dissipation and vibration reduction effect of the concrete structure.

(2) The stator foundation measurement point and the lower frame foundation measurement point together characterize the vibration of the turbine pier, and the top cover characterizes the vibration of the tailwater pipe. Under different working conditions, the transmission path of vibration caused by tailwater fluctuation between each measurement point is unchanged, indicating that the change in the operating state of the hydropower station unit does not affect the transmission direction of vibration signal. According to the transfer-entropy curve and information-transmission rate between different measurement points, the transmission law of tailwater fluctuation vibration is judged as follows: tailwater pipe (top cover measurement point)→turbine pier (stator foundation measurement point, lower frame foundation measurement point)→generator floor (generator floor measurement point).

(3) The lower frame foundation is an important support structure of the hydropower house, and the maximum information-transmission rate can be obtained between the top cover and the lower frame foundation under different working conditions,

indicating that the lower frame foundation is the main node of tailwater-fluctuation transmission in the hydropower house.

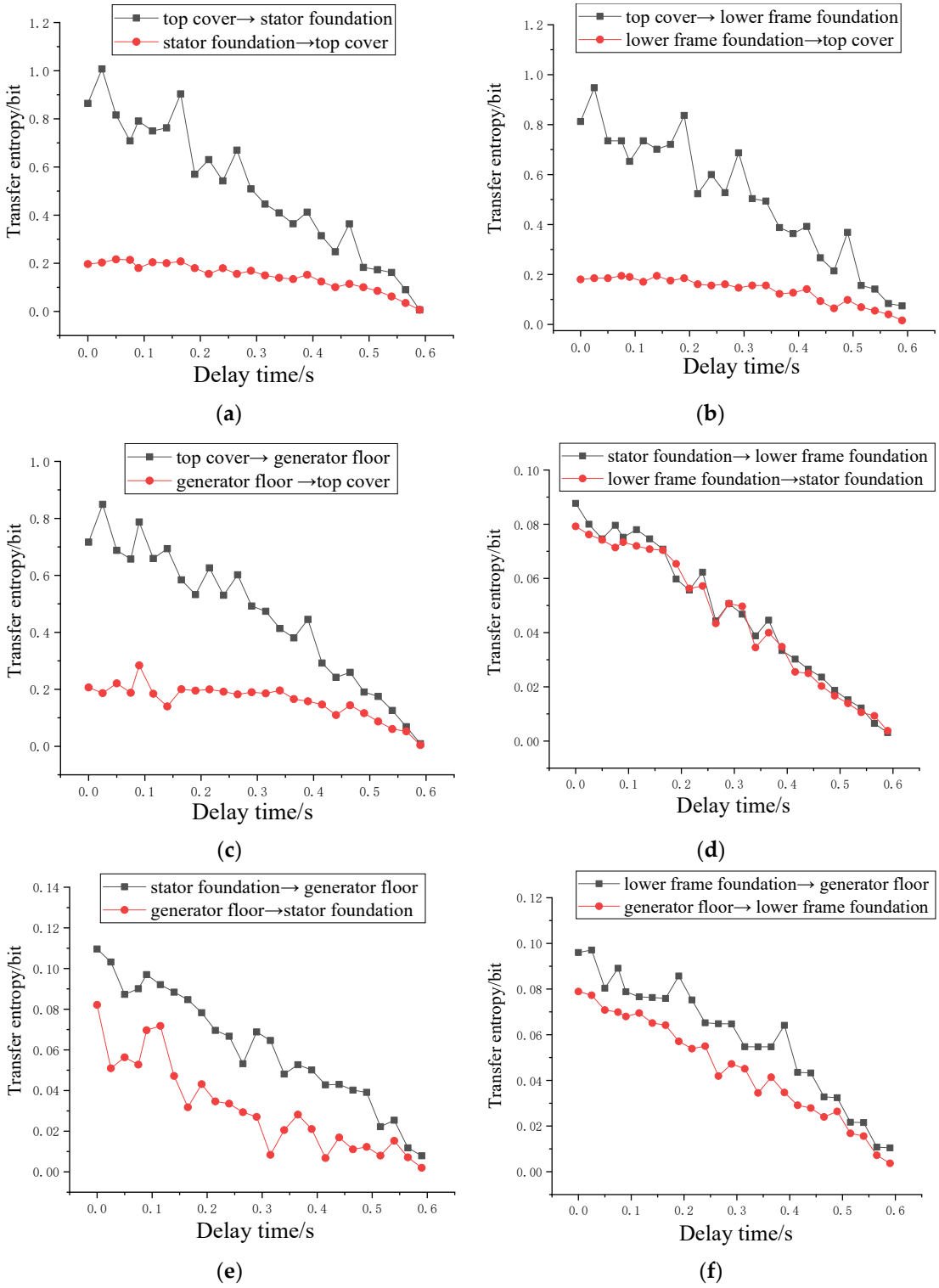

Figure 16. Transfer-entropy curve between measurement points of condition 3. (**a**) Transfer-entropy curve of top cover and stator foundation; (**b**) Transfer-entropy curve of top cover and lower frame foundation; (**c**) Transfer-entropy curve of top cover and generator floor; (**d**) Transfer-entropy curve of stator foundation and lower frame foundation; (**e**) Transfer-entropy curve of stator foundation and generator floor; (**f**) Transfer-entropy curve of lower frame foundation and generator floor.

Table 7. Information-transmission rate between the main measurement points under three conditions.

Transmission Direction	Top Cover→Stator Foundation	Top Cover→Lower Frame Foundation	Stator Foundation→Generator Floor	Lower Frame Foundation→Generator Floor
Condition 1	91.54	94.86	32.85	32.78
Condition 2	64.72	82.19	73.95	55.23
Condition 3	71.67	72.99	47.62	29.97

5. Conclusions

This paper explores a vibration-transmission-path identification method based on CEEMDAN-SVD-TE, verifies the effectiveness of the algorithm through simulation signal analysis, analyzes the vibration-transmission path caused by tailwater fluctuation of the Quxue hydropower house, and obtains the following conclusions:

(1) The transfer-entropy (TE) algorithm, as a method for judging the information-transmission effect between signals, can effectively identify the source of information transmission, but the results of this algorithm are easily affected by noise; CEEMDAN-SVD, as a secondary filtering signal-processing approach, can retain the useful information in the signal and filter out the noise effectively. The innovative combination of CEEMDAN-SVD and TE method can give full use to the advantages of each method and obtain accurate and true information-transmission paths.

(2) The transmission path identification method of CEEMDAN-SVD-TE provides a new method and innovative perspective for the analysis of vibration response and vibration mechanism in hydraulic structures. Based on CEEMDAN-SVD-TE, the vibration response due to tailwater fluctuation was analyzed, and it was found that the vibration-transmission path of the hydropower house under different working conditions is tailwater pipe (top cover measurement point)→turbine pier (stator foundation measurement point, lower frame foundation measurement point)→generator floor (generator floor measurement point).

(3) Combining all the identified transmission paths under the three operating conditions, it can be found that the lower frame foundation is transmitted the largest amount of information, while the least amount of vibration information is transferred through the lower frame foundation. This indicates that the lower frame foundation, as the main load-bearing member of the hydropower house, is an important node in the vibration-transmission of the house and a key factor for the optimal design of vibration isolation in the hydropower house.

(4) On the basis of the signal generated by the vibration response, this paper analyzes the transmission pattern of the hydropower house, which not only identifies the transmission path of vibration in the hydropower house, but also quantitatively describes the transmission feature of the vibration information. The vibration-transmission path based on the CEEMDAN-SVD-TE method can provide a theoretical basis for the identification of vibration-transmission paths in a hydropower house, offer an essential reference for the optimal designing and damping of the house and suggest a new idea for structural vibration monitoring and safety management of hydropower stations.

Author Contributions: Conceptualization, J.Z.; methodology, Z.L. and M.C.; validation, Z.L. and M.C.; formal analysis, Z.L. and M.C.; investigation, M.C. and Z.L.; resources, J.Z.; data curation, Z.L. and M.C.; writing—original draft preparation, Z.L.; writing—review and editing, J.Z., Z.L., H.L. and J.H.; visualization, Z.L.; supervision, J.Z., Z.L. and J.H. All authors have read and agreed to the published version of the manuscript.

Funding: This work is supported by the National Natural Science Foundation of China (51679091), the Program for Water Conservancy Science and Technology Innovation Project in Guangdong Province (2020-18) and the Innovative Project of North China University of Water Resources and Electric power (YK-2021-30).

Institutional Review Board Statement: Not applicable.

Informed Consent Statement: Not applicable.

Data Availability Statement: Not applicable.

Conflicts of Interest: The authors declare no conflict of interest.

References

1. Li, M.; He, N. Carbon intensity of global existing and future hydropower reservoirs. *Renew. Sust. Energy Rev.* **2022**, *162*, 112433. [CrossRef]
2. Daneshgar, S.; Zahedi, R. Investigating the hydropower plants production and profitability using system dynamics approach. *J. Energy Storage* **2022**, *46*, 103919. [CrossRef]
3. Zhang, Y.; Ma, H.; Zhao, S. Assessment of hydropower sustainability: Review and modeling. *J. Clean. Prod.* **2021**, *321*, 128898. [CrossRef]
4. Kumar, K.; Saini, R.P. A review on operation and maintenance of hydropower plants. *Sustain. Energy Technol. Assess.* **2022**, *49*, 101704. [CrossRef]
5. Zhao, Y.; Feng, J.; Li, Z.; Dang, M.; Luo, X. Analysis of Pressure Fluctuation of Tubular Turbine under Different Application Heads. *Sustainability* **2022**, *14*, 5133. [CrossRef]
6. Xu, B.; Luo, X.; Egusquiza, M.; Ye, W.; Liu, J.; Egusquiza, E.; Chen, D.; Guo, P. Nonlinear modal interaction analysis and vibration characteristics of a francis hydro-turbine generator unit. *Renew. Energy* **2021**, *168*, 854–864. [CrossRef]
7. Liming, Z.; Yongyao, L.; Zhengwei, W.; Xin, L.; Yexiang, X. A review on the large tilting pad thrust bearings in the hydropower units. *Renew. Sust. Energy Rev.* **2017**, *69*, 1182–1198. [CrossRef]
8. Wu, Q.; Zhang, L.; Ma, Z. A model establishment and numerical simulation of dynamic coupled hydraulic–mechanical–electric–structural system for hydropower station. *Nonlinear. Dynam.* **2017**, *87*, 459–474. [CrossRef]
9. Wu, Q.; Zhang, L.; Ma, Z.; Wang, X. Vibration characteristics of the unit-plant structure of a hydropower station under transient load-up process. *J. Vib. Shock.* **2019**, *38*, 53–61.
10. Tang, X.; Hu, B.; Wen, H. Fault Diagnosis of Hydraulic Generator Bearing by VMD-Based Feature Extraction and Classification. *Iran. J. Sci. Technol. Trans. Electr. Eng.* **2021**, *45*, 1227–1237. [CrossRef]
11. Same, M.H.; Gandubert, G.; Gleeton, G.; Ivanov, P.; Landry, R., Jr. Simplified welch algorithm for spectrum monitoring. *Appl. Sci.* **2020**, *11*, 86. [CrossRef]
12. Liu, Q.; Wang, Y.; Xu, Y. Synchrosqueezing extracting transform and its application in bearing fault diagnosis under non-stationary conditions. *Measurement* **2021**, *173*, 108569. [CrossRef]
13. Crochiere, R.; Rabiner, L. Optimum FIR digital filter implementations for decimation, interpolation, and narrow-band filtering. *IEEE Trans. Acous. Speech. Signal. Pr.* **1975**, *23*, 444–456. [CrossRef]
14. Pilipović, R.; Risojević, V.; Bulić, P. On the design of an energy efficient digital IIR A-weighting filter using approximate multiplication. *Sensors* **2021**, *21*, 732. [CrossRef] [PubMed]
15. Cao, Y.; Liu, M.; Yang, J.; Cao, Y.; Fu, W. A method for extracting weak impact signal in NPP based on adaptive Morlet wavelet transform and kurtosis. *Prog. Nucl. Energy* **2018**, *105*, 211–220. [CrossRef]
16. Huang, N.E.; Shen, Z.; Long, S.R.; Wu, M.C.; Shih, H.H.; Zheng, Q.; Yen, N.-C.; Tung, C.C.; Liu, H.H. The empirical mode decomposition and the Hilbert spectrum for nonlinear and non-stationary time series analysis. *Proc. R. Soc. Lond. Ser. A Math. Phys. Eng. Sci.* **1998**, *454*, 903–995. [CrossRef]
17. Huang, N.E.; Shen, Z.; Long, S.R. A new view of nonlinear water waves: The Hilbert spectrum. *Annu. Rev. Fluid Mech.* **1999**, *31*, 417–457. [CrossRef]
18. Barbosh, M.; Singh, P.; Sadhu, A. Empirical mode decomposition and its variants: A review with applications in structural health monitoring. *Smart Mater. Struct.* **2020**, *29*, 093001. [CrossRef]
19. Bolaers, F.; Cousinard, O.; Estocq, P.; Chiementin, X.; Dron, J.P. Comparison of denoising methods for the early detection of fatigue bearing defects by vibratory analysis. *J. Vib. Control* **2011**, *17*, 1983–1993. [CrossRef]
20. Liu, M.D.; Ding, L.; Bai, Y.L. Application of hybrid model based on empirical mode decomposition, novel recurrent neural networks and the ARIMA to wind speed prediction. *Energy Convers. Manag.* **2021**, *233*, 113917. [CrossRef]
21. Wu, Z.; Huang, N.E. Ensemble empirical mode decomposition: A noise-assisted data analysis method. *Adv. Adapt. Data Anal.* **2009**, *1*, 1–41. [CrossRef]
22. Spinosa, E.; Iafrati, A. A noise reduction method for force measurements in water entry experiments based on the Ensemble Empirical Mode Decomposition. *Mech. Syst. Signal Pr.* **2022**, *168*, 108659. [CrossRef]
23. Gao, Z.; Liu, Y.; Wang, Q.; Wang, J.; Luo, Y. Ensemble empirical mode decomposition energy moment entropy and enhanced long short-term memory for early fault prediction of bearing. *Measurement* **2022**, *188*, 110417. [CrossRef]
24. Wang, H.; Liu, Z.; Song, Y.; Lu, X. Ensemble EMD-based signal denoising using modified interval thresholding. *IET. Signal Process.* **2017**, *11*, 452–461. [CrossRef]
25. Kuai, M.; Cheng, G.; Pang, Y.; Li, Y. Research of planetary gear fault diagnosis based on permutation entropy of CEEMDAN and ANFIS. *Sensors* **2018**, *18*, 782. [CrossRef]

26. Chen, W.; Li, J.; Wang, Q.; Han, K. Fault feature extraction and diagnosis of rolling bearings based on wavelet thresholding denoising with CEEMDAN energy entropy and PSO-LSSVM. *Measurement* **2021**, *172*, 108901. [CrossRef]
27. Mousavi, A.A.; Zhang, C.; Masri, S.F.; Gholipour, G. Structural damage detection method based on the complete ensemble empirical mode decomposition with adaptive noise: A model steel truss bridge case study. *Struct. Health Monit.* **2022**, *21*, 887–912. [CrossRef]
28. Zhang, J.; Hou, G.; Ma, B.; Hua, W. Operating characteristic information extraction of flood discharge structure based on complete ensemble empirical mode decomposition with adaptive noise and permutation entropy. *J. Vib. Control* **2018**, *24*, 5291–5301. [CrossRef]
29. Cheng, X.; Mao, J.; Li, J.; Zhao, H.; Zhou, C.; Gong, X.; Rao, Z. An EEMD-SVD-LWT algorithm for denoising a lidar signal. *Measurement* **2021**, *168*, 108405. [CrossRef]
30. Xu, W.; Ma, Z. Study of the vibration transmission and path recognition of an underground powerhouse using energy finite element method. *Shock. Vib.* **2016**, *2016*, 5039578. [CrossRef]
31. Lian, J.; Wang, H.; Wang, H. Study on vibration transmission among units in underground powerhouse of a hydropower station. *Energies* **2018**, *11*, 3015. [CrossRef]
32. Wang, H.; Tu, K.; Lian, J. Research on transfer path of vibrations of hydropower house based on structural intensity. *J. Hydraul. Eng.* **2015**, *46*, 1247–1252.
33. Lindner, B.; Auret, L.; Bauer, M.; Groenewald, J.W. Comparative analysis of Granger causality and transfer entropy to present a decision flow for the application of oscillation diagnosis. *J. Process. Contr.* **2019**, *79*, 72–84. [CrossRef]
34. Wang, P.; Deng, Y.; Li, H.; Chen, D. Making connections: Information transfer in hydropower generation system during the transient process of load rejection. *Sustain. Energy Technol. Assess.* **2022**, *50*, 101766. [CrossRef]
35. Wang, H.; Wang, N.; Lian, J. Vibration transfer path identification of the hydropower house based on transfer entropy. *J. Hydraul. Eng.* **2018**, *49*, 732–740.
36. Zhang, L.; Wang, S.; Yin, G.; Guan, C. Vibration transmission path identification in a hydropower house based on a time-delayed transfer entropy method. *J. Vib. Control* **2020**, *26*, 1214–1227. [CrossRef]
37. Wang, Q.; Wang, L.; Yu, H.; Wang, D.; Nandi, A.K. Utilizing SVD and VMD for Denoising Non-Stationary Signals of Roller Bearings. *Sensors* **2021**, *22*, 195. [CrossRef]
38. Schreiber, T. Measuring information transfer. *Phys. Rev. Lett.* **2000**, *85*, 461. [CrossRef]
39. Nichols, J.M. Examining structural dynamics using information flow. *Probabilist. Eng. Mech.* **2006**, *21*, 420–433. [CrossRef]
40. Overbey, L.A.; Todd, M.D. Dynamic system change detection using a modification of the transfer entropy. *J. Sound. Vib.* **2009**, *322*, 438–453. [CrossRef]